

Strong coupling phases of the anisotropic Kardar-Parisi-Zhang equation

Thomas Kloss¹, Léonie Canet^{2,3}, and Nicolás Wschebor⁴

¹*IIP, Universidade Federal do Rio Grande do Norte, Av. Odilon Gomes de Lima 1722, 59078-400 Natal, Brazil*

²*Université Grenoble Alpes, UMR 5493, LPMMC, F-38000 Grenoble, France*

³*CNRS, UMR 5493, LPMMC, F-38000 Grenoble, France*

⁴*Instituto de Física, Facultad de Ingeniería, Universidad de la República, J.H.y Reissig 565, 11000 Montevideo, Uruguay*

(Dated: September 26, 2014)

We study the anisotropic Kardar-Parisi-Zhang equation using nonperturbative renormalization group methods. In contrast to a previous analysis in the weak-coupling regime we find the strong coupling fixed point corresponding to the isotropic rough phase to be always locally stable and unaffected by the anisotropy even at non-integer dimensions. Apart from the well-known weak-coupling and the now well established isotropic strong coupling behavior, we find an anisotropic strong coupling fixed point for nonlinear couplings of opposite signs at non-integer dimensions.

PACS numbers: 05.10.Cc,64.60.Ht,68.35.Ct,68.35.Rh

I. INTRODUCTION

The Kardar-Parisi-Zhang (KPZ) equation [1–4], originally intended to describe growing interfaces, has become a paradigm for kinetic roughening and dynamical scaling phenomena. Apart from its relevance in statistical physics a connection to condensed matter systems has also been established recently [5, 6]. A variant of the original KPZ model, namely the anisotropic Kardar-Parisi-Zhang (AKPZ) equation was introduced some years later in the 90s by Villain and Wolf [7, 8], aiming at describing vicinal surfaces and the effect of anisotropy. Being for a long time more a subject of academic interest and much less studied than the standard KPZ model, the AKPZ equation has also experienced recently an unexpected relevance in condensed matter systems. It was shown by Chen and coworkers that the order parameter for the dynamics of a driven Bose-Einstein condensate maps onto a compact form of the AKPZ equation [9, 10]. In contrast to the standard KPZ equation however, where thanks to an exact solution in one dimension [11–17] and extensive simulations in higher dimensions [18–28] the phase diagram is relatively well understood, much less effort was spent on the AKPZ equation and most of the studies are limited to the weak-coupling regime [8, 29–33]. An understanding of the AKPZ equation which includes the strong-coupling behavior was missing until now.

The AKPZ equation supposes the d -dimensional space to be partitioned into two orthogonal and isotropic subspaces with dimensions d_{\perp} and d_{\parallel} . In the original work by Wolf [8] where the dimensions of the two sectors were chosen equally ($d_{\parallel} = d_{\perp} = 1$) so that the total dimension is $d = 2$, the anisotropy is found to be only of minor importance and basically leading to the same universality classes as the isotropic KPZ equation. That is, if both couplings were chosen with an equal sign, the isotropic KPZ behavior was recovered at long distances whereas in the case of an opposite sign or with one vanishing coupling the weak-coupling Edwards-Wilkinson (EW) behavior with logarithmic roughness was obtained. The results of Wolf were confirmed by numerical simulations

[34–36] and the logarithmic correlations by exact arguments [37]. In contrast, studies on variants of the KPZ equation [38–42] as well as on related models [43, 44] indicated that anisotropy may become important in some cases. A subsequent study of the AKPZ equation performed by Täuber and Frey (TF) [29] by means of dynamic renormalization group later revealed that the result of Wolf is only a special case and the situation in generic dimension is more complex. Depending on the total dimension d and on the splitting in the two sector dimensions d_{\parallel} and d_{\perp} , TF argued that the anisotropy can lead not only to new universality classes but may also cause the isotropic solution to become unstable.

In the present study, we reexamine the AKPZ equation by means of nonperturbative renormalization group (NPRG) methods. The NPRG approach to the KPZ equation was developed in [45–48]. It successfully yields the KPZ phase diagram with the correct strong coupling behavior and the corresponding exponents are in close agreement with simulation results in $d = 2$ and $d = 3$. In $d = 1$ the exact exponents are recovered and the scaling function of the height-height correlations compares very accurately with the exact scaling function from Ref. [11]. Throughout this work we use two different approximations: the simpler local-potential prime approximation (LPA') [49] to obtain the phase diagram and the more accurate Next-to-Leading Order (NLO) approximation of Ref. [47] in order to check our findings. The LPA' approximation does not lead to accurate numbers for the exponents but in general it reproduces qualitatively the phase diagram with the correct strong coupling behavior. A similar strategy with these two approximations has recently been successfully used to study the KPZ equation with Gaussian long-range correlated noise [48].

As shown by TF, the stability of the weak-coupling isotropic EW fixed point as well as of the weak-coupling uniaxial (EWU) fixed point are changed when a third weak-coupling anisotropic (EWA) fixed point is crossing them. This happens in certain dimension combinations. They conjectured that the instability of the EW fixed point against anisotropic perturbations would indi-

cate the instability of the whole isotropic KPZ equation against anisotropic perturbations. TF further speculated that a finite upper critical dimension may result from this instability. Our analysis of the NPRG flow equations however shows that no prediction for the strong-coupling behavior can be drawn from the stability changes in the weak-coupling sector. In the weak coupling regime, our results are in close agreement with the ones by TF and we recover the same fixed points with the predicted stability changes. In addition to the weak coupling regime, the NPRG approach also describes the strong coupling behavior with the isotropic rough phase, characterized by a fully attractive strong coupling (SC) fixed point. If both initial nonlinear couplings are chosen with a equal sign (and, in the case $d > 2$ sufficiently large) the isotropic strong-coupling fixed point is always reached. That is, we find that the stability change of the isotropic EW fixed point, triggered by the crossing EWA fixed point does not affect the isotropic strong-coupling fixed point. In our scenario the isotropic rough phase is always locally stable for an arbitrary splitting in the two sector dimensions. If the initial nonlinear couplings are chosen with opposite signs or if one of them is zero (the uniaxial case) additional strong-coupling fixed points are found in some cases. We observe however, that these fixed points do not enter in the quadrant where both couplings have the same sign and therefore never cross the isotropic strong-coupling fixed point to change its stability.

The paper is organized as follows. In Sec. II, we shortly present the NPRG formalism for the AKPZ equation, our ansatz with the approximations used and the corresponding flow equations. In Sec. III the fixed point solutions of the flow equations are presented and the full phase diagram of the system is determined. The results are summarized in Sec. IV. Technical details and the connection to the results by TF can be found in the appendices.

II. METHOD

A. AKPZ field theory

The AKPZ equation [8] reads

$$\begin{aligned} \frac{\partial h(t, \vec{x})}{\partial t} &= \nu_{\parallel} \nabla_{\parallel}^2 h(t, \vec{x}) + \nu_{\perp} \nabla_{\perp}^2 h(t, \vec{x}) \\ &+ \frac{\lambda_{\parallel}}{2} (\nabla_{\parallel} h(t, \vec{x}))^2 + \frac{\lambda_{\perp}}{2} (\nabla_{\perp} h(t, \vec{x}))^2 + \eta(t, \vec{x}), \end{aligned} \quad (1)$$

where $h(t, \vec{x}) \equiv h(t, \vec{x}_{\parallel}, \vec{x}_{\perp})$ is a single valued height profile which depends on the spatial substrate coordinates $\vec{x} = (\vec{x}_{\parallel}, \vec{x}_{\perp})^T$ and on time t . Parallel and perpendicular components of the substrate have dimensions d_{\parallel} and d_{\perp} in each sector so that the total substrate dimension is $d = d_{\parallel} + d_{\perp}$. The AKPZ equation has two surface-tension terms and two non-linear couplings proportional to ν_i and λ_i with $i = \{\parallel, \perp\}$. The last term $\eta(t, \vec{x})$ represents the noise. As in Refs. [8, 29] we choose Gaussian

white noise with zero mean $\langle \eta(t, \vec{x}) \rangle = 0$ and the isotropic correlator

$$\langle \eta(t, \vec{x}) \eta(t', \vec{x}') \rangle = 2D \delta^{(d_{\parallel})}(\vec{x}_{\parallel} - \vec{x}'_{\parallel}) \delta^{(d_{\perp})}(\vec{x}_{\perp} - \vec{x}'_{\perp}) \delta(t - t'), \quad (2)$$

where D is the noise amplitude. A field theory can be obtained in the usual way with the Janssen-de Dominicis procedure [50], introducing an additional Martin-Siggia-Rose response field \tilde{h} [51]. Eq. (1) is thereby expressed as the functional integral

$$\begin{aligned} \mathcal{Z}[j, \tilde{j}] &= \int \mathcal{D}[h, \tilde{h}] \exp\left(-\mathcal{S}[h, \tilde{h}] + \int_{\mathbf{x}} \{j h + \tilde{j} \tilde{h}\}\right), \quad (3a) \\ \mathcal{S}[h, \tilde{h}] &= \int_{\mathbf{x}} \left\{ \tilde{h}(\mathbf{x}) (\partial_t h(\mathbf{x}) - \nu_{\parallel} \nabla_{\parallel}^2 h(\mathbf{x}) - \nu_{\perp} \nabla_{\perp}^2 h(\mathbf{x}) \right. \\ &\quad \left. - \frac{\lambda_{\parallel}}{2} (\nabla_{\parallel} h(\mathbf{x}))^2 - \frac{\lambda_{\perp}}{2} (\nabla_{\perp} h(\mathbf{x}))^2 - D(\tilde{h}(\mathbf{x}))^2 \right\}, \end{aligned} \quad (3b)$$

where j and \tilde{j} are sources and we have introduced the notation $\mathbf{x} \equiv (t, \vec{x}_{\parallel}, \vec{x}_{\perp})$ for convenience. For later reference, we also write frequency and momentum labels as $\mathbf{q} \equiv (\omega, \vec{q}_{\parallel}, \vec{q}_{\perp})$ and use the Fourier transform convention of Ref. [47] throughout this work. Being only of technical relevance and without loss of generality, we work in the following with the rescaled AKPZ action, such that $\nu_{\parallel} = \nu_{\perp}$, see appendix B.

The AKPZ action Eq. (3b) is invariant under both infinitesimal field transformations

$$(i) \begin{cases} h'(t, \vec{x}) = \vec{x} \cdot \partial_t \vec{v}(t) + h(t, \vec{x} + \langle \vec{\lambda}, \vec{v}(t) \rangle) \\ \tilde{h}'(t, \vec{x}) = \tilde{h}(t, \vec{x} + \langle \vec{\lambda}, \vec{v}(t) \rangle) \end{cases} \quad (4a)$$

$$(ii) \quad h'(t, \vec{x}) = h(t, \vec{x}) + c(t). \quad (4b)$$

with $\vec{v} \equiv (\vec{v}_{\parallel}, \vec{v}_{\perp})^T$ and $\langle \vec{\lambda}, \vec{v} \rangle \equiv (\lambda_{\parallel} \vec{v}_{\parallel}, \lambda_{\perp} \vec{v}_{\perp})^T$ up to some terms which variations are linear in the fields. Relation (i) corresponds to the Galilean symmetry in a time-gauged form [46, 52] and (ii) is the shift symmetry also gauged in time. As in these references, Ward identities can be deduced from them. These symmetries constitute the central elements to device our NPRG ansatz in Sec. II C. Note that the Cole-Hopf version of the AKPZ action with the related Z_2 symmetry holds only in the specific case of $\nu_{\perp} \lambda_{\perp} / (\nu_{\perp} \lambda_{\parallel}) = 1$ as pointed out in Ref. [8]. Contrarily to the isotropic situation, there is no time reversal symmetry [45, 53] in the anisotropic case. In the symmetric case where $\nu_{\parallel} = \nu_{\perp}$ and $\lambda_{\parallel} = \lambda_{\perp}$ an additional rotational symmetry is present and the AKPZ action identifies with the isotropic one. In the uniaxial case with $\lambda_{\perp} = 0$ an additional symmetry exists and this implies that the hypersurface $\gamma = 0$ is closed along the flow. To the best of our knowledge this symmetry has not yet been discussed elsewhere in the literature. We refer to appendix E for further details.

B. Nonperturbative renormalization group

The NPRG can be seen as a generalization of Wilson's idea to construct an effective field theory for the long-range physics by continuously integrating out fast degrees of freedom. We do not go into details here and only highlight the main steps. We refer the reader to Refs. [49, 54, 55] for a general introduction to the NPRG. Applications of the NPRG method to describe out-of-equilibrium situations can be found e.g. in Refs. [56–59] and the first application to the KPZ problem is achieved in Ref. [45]. The starting point in a NPRG description is to add a regulator term

$$\Delta\mathcal{S}_\kappa = \frac{1}{2} \int_{\mathbf{q}} h_i(-\mathbf{q}) [R_\kappa(\mathbf{q})]_{ij} h_j(\mathbf{q}), \quad (5)$$

to the action Eq. (3b), where $i, j \in \{1, 2\}$ label the field and response field $h_1 = h, h_2 = \tilde{h}$. R_κ is the regulator matrix and κ is a running cutoff. Since the action is now cutoff dependent the partition function

$$\mathcal{Z}_\kappa[j, \tilde{j}] = \int \mathcal{D}[h, \tilde{h}] \exp\left(-\mathcal{S} - \Delta\mathcal{S}_\kappa + \int_{\mathbf{x}} \{jh + \tilde{j}\tilde{h}\}\right) \quad (6)$$

depends on the external scale κ . The form of the regulator is quite general but its asymptotic behavior must fulfill some requirements. For $\kappa \gg q$ the regulator behaves like a mass with $R_\kappa \sim \kappa^2$ so that all fluctuations are suppressed in the limit $\kappa \rightarrow \infty$. Lowering the cutoff down to $\kappa \ll q$ the cutoff function vanishes, so that in the limit $\kappa \rightarrow 0$ the original theory without regulator is recovered. We choose the regulator function as

$$R_\kappa(\mathbf{q}) = r \left(\frac{q^2}{\kappa^2} \right) \begin{pmatrix} 0 & \nu_\kappa^\parallel q_\parallel^2 + \nu_\kappa^\perp q_\perp^2 \\ \nu_\kappa^\parallel q_\parallel^2 + \nu_\kappa^\perp q_\perp^2 & -2D_\kappa \end{pmatrix}, \quad (7)$$

with $q_i = |\vec{q}_i|$ where $i = \{\parallel, \perp\}$ such that it preserves all the symmetries of the AKPZ action. The scale dependent parameters $\nu_\kappa^\parallel, \nu_\kappa^\perp$ and D_κ , are defined later in Eqs. (26,34). We use an exponential cutoff function of the form

$$r(x) = \alpha / (\exp(x) - 1). \quad (8)$$

where α is a free parameter, which can be varied to assess the quality of an approximation. Unless otherwise indicated, we choose $\alpha = 4$ throughout this work since the variations of the critical exponents are minimal around this value for $d = 2, 3$ [48]. Defining the functional $\mathcal{W}_\kappa = \log \mathcal{Z}_\kappa$, field expectation values are obtained as functional derivatives with respect to the sources j and \tilde{j}

$$\varphi(\mathbf{x}) = \langle h(\mathbf{x}) \rangle = \frac{\delta \mathcal{W}_\kappa}{\delta j(\mathbf{x})}, \quad \tilde{\varphi}(\mathbf{x}) = \langle \tilde{h}(\mathbf{x}) \rangle = \frac{\delta \mathcal{W}_\kappa}{\delta \tilde{j}(\mathbf{x})}. \quad (9)$$

The effective action $\Gamma_\kappa[\varphi, \tilde{\varphi}]$ is defined as

$$\Gamma_\kappa[\varphi, \tilde{\varphi}] + \mathcal{W}_\kappa[j, \tilde{j}] = \int j_i \varphi_i - \frac{1}{2} \int \varphi_i [R_\kappa]_{ij} \varphi_j, \quad (10)$$

which is up to a term proportional to R_κ the Legendre transform of \mathcal{W}_κ . The exact flow for $\Gamma_\kappa[\varphi, \tilde{\varphi}]$ is given by Wetterich's equation, which reads in Fourier space [49, 54, 55, 60]

$$\partial_\kappa \Gamma_\kappa = \frac{1}{2} \text{Tr} \int_{\mathbf{q}} \partial_\kappa R_\kappa \cdot G_\kappa, \quad (11)$$

and where

$$G_\kappa = \left[\Gamma_\kappa^{(2)} + R_\kappa \right]^{-1}, \quad (12)$$

is the full propagator in presence of external fields.

C. Ansatz

Our aim is to build an approximation scheme for the AKPZ equation, which automatically preserves along the flow the symmetries of the problem, summarized in Eq. (4). The strategy which is inspired from Refs. [61, 62] and is similar to the approach used in Ref. [46] for the isotropic KPZ equation, is to construct an ansatz in terms of symmetry invariant building blocks. In the AKPZ equation these invariant blocks are the covariant time derivative of the field

$$D_t \varphi = \partial_t \varphi - \frac{\lambda_\parallel}{2} (\nabla_\parallel \varphi)^2 - \frac{\lambda_\perp}{2} (\nabla_\perp \varphi)^2, \quad (13)$$

and the Galilean invariants $\tilde{\varphi}, \nabla_\parallel^2 \varphi, \nabla_\perp^2 \varphi$ and gradients and appropriate covariant time derivatives of them. In order to keep the full momentum dependence of the 2-point functions, we further introduce four running functions $f_\kappa^X(\vec{p})$ with $X \in \{\lambda, D, \nu_\parallel, \nu_\perp\}$. In principle, these running functions also depend on the frequency like in Ref. [46]. However, to preserve the anisotropic momentum dependence while keeping the equations numerically tractable, we use the next-to-leading order (NLO) approximation of Ref. [47]. It consists in neglecting the frequency dependence of the four flowing functions $f_\kappa^X(\omega, \vec{p}) \rightarrow f_\kappa^X(\vec{p})$ within the loop integrals which reduces drastically the numerical complexity. In the isotropic case, this approximation is reliable typically up to $d \lesssim 3.5$, as can be inferred from the dependence of the exponents in the cutoff parameter α , see [47]. The NLO ansatz reads

$$\Gamma_\kappa[\varphi, \tilde{\varphi}] = \int_{\mathbf{x}} \left\{ \tilde{\varphi} f_\kappa^\lambda(\nabla) D_t \varphi - (\nabla_\parallel^2 \varphi) f_\kappa^{\nu_\parallel}(\nabla) \tilde{\varphi} - (\nabla_\perp^2 \varphi) f_\kappa^{\nu_\perp}(\nabla) \tilde{\varphi} - \tilde{\varphi} f_\kappa^D(\nabla) \varphi \right\}, \quad (14)$$

with $f_\kappa^X(\nabla) \equiv f_\kappa^X(-\nabla_\parallel^2, -\nabla_\perp^2)$. Taking functional derivatives of the ansatz w.r.t. φ and $\tilde{\varphi}$ and evaluating them at $\varphi = \tilde{\varphi} = 0$ we obtain for the 2-point functions

$$\Gamma_\kappa^{(2,0)}(\omega, \vec{p}_\parallel, \vec{p}_\perp) = 0, \quad (15a)$$

$$\Gamma_\kappa^{(1,1)}(\omega, \vec{p}_\parallel, \vec{p}_\perp) = i\omega f_\kappa^\lambda(p_\parallel, p_\perp) + \vec{p}_\parallel^2 f_\kappa^{\nu_\parallel}(p_\parallel, p_\perp) + \vec{p}_\perp^2 f_\kappa^{\nu_\perp}(p_\parallel, p_\perp), \quad (15b)$$

$$\Gamma_\kappa^{(0,2)}(\omega, \vec{p}_\parallel, \vec{p}_\perp) = -2f_\kappa^D(p_\parallel, p_\perp). \quad (15c)$$

Further, we make the approximation

$$f_{\kappa}^{\nu\perp}(p_{\parallel}, p_{\perp}) = \gamma_{\kappa}^{-1} f_{\kappa}^{\nu\parallel}(p_{\parallel}, p_{\perp}), \quad (16)$$

where $\gamma_{\kappa} = \nu_{\kappa}^{\parallel}/\nu_{\kappa}^{\perp}$ and use the notation $f_{\kappa}^{\nu\parallel} \equiv f_{\kappa}^{\nu}$ for convenience. We are left with three flowing functions f_{κ}^X where $X \in \{\lambda, D, \nu\}$. These functions are extracted from the 2-point functions as

$$f_{\kappa}^{\nu}(p_{\parallel}, p_{\perp}) = \frac{1}{\vec{p}_{\parallel}^2 + \gamma_{\kappa}^{-1} \vec{p}_{\perp}^2} \Re \Gamma_{\kappa}^{(1,1)}(\omega, \vec{p}_{\parallel}, \vec{p}_{\perp}) \Big|_{\omega=0} \quad (17a)$$

$$f_{\kappa}^{\lambda}(p_{\parallel}, p_{\perp}) = \frac{1}{\omega} \Im \Gamma_{\kappa}^{(1,1)}(\omega, \vec{p}_{\parallel}, \vec{p}_{\perp}) \Big|_{\omega=0}, \quad (17b)$$

$$f_{\kappa}^D(p_{\parallel}, p_{\perp}) = -\frac{1}{2} \Gamma_{\kappa}^{(0,2)}(\omega, \vec{p}_{\parallel}, \vec{p}_{\perp}) \Big|_{\omega=0}. \quad (17c)$$

From Eqs. (7,12,15) the propagator follows as

$$G_{\kappa}(\omega, \vec{q}_{\parallel}, \vec{q}_{\perp}) = \frac{1}{P_{\kappa}(\omega, q)} \begin{pmatrix} 2k_{\kappa}(q) & Y_{\kappa}(\omega, q_{\parallel}, q_{\perp}) \\ Y_{\kappa}^*(\omega, q_{\parallel}, q_{\perp}) & 0 \end{pmatrix}, \quad (18)$$

where

$$k_{\kappa}(q_{\parallel}, q_{\perp}) = f_{\kappa}^D(q_{\parallel}, q_{\perp}) + D_{\kappa} r(q^2/\kappa^2), \quad (19a)$$

$$l_{\kappa}(q_{\parallel}, q_{\perp}) = q_{\parallel}^2 (f_{\kappa}^{\nu}(q_{\parallel}, q_{\perp}) + \nu_{\kappa}^{\parallel} r(q^2/\kappa^2)) + q_{\perp}^2 (f_{\kappa}^{\nu}(q_{\parallel}, q_{\perp}) + \nu_{\kappa}^{\perp} r(q^2/\kappa^2)), \quad (19b)$$

$$Y_{\kappa}(\omega, q_{\parallel}, q_{\perp}) = i\omega f_{\kappa}^{\lambda}(q_{\parallel}, q_{\perp}) + l_{\kappa}(q_{\parallel}, q_{\perp}), \quad (19c)$$

$$P_{\kappa}(\omega, q_{\parallel}, q_{\perp}) = (\omega f_{\kappa}^{\lambda}(q_{\parallel}, q_{\perp}))^2 + (l_{\kappa}(q_{\parallel}, q_{\perp}))^2. \quad (19d)$$

The scale derivative of the regulator matrix Eq. (7) is

$$\partial_{\kappa} R_{\kappa}(\vec{q}) = \begin{pmatrix} 0 & q_{\parallel}^2 \partial_{\kappa} S_{\kappa}^{\parallel}(q) + q_{\perp}^2 \partial_{\kappa} S_{\kappa}^{\perp}(q) \\ q_{\parallel}^2 \partial_{\kappa} S_{\kappa}^{\parallel}(q) + q_{\perp}^2 \partial_{\kappa} S_{\kappa}^{\perp}(q) & -2\partial_{\kappa} S_{\kappa}^D(q) \end{pmatrix}, \quad (20)$$

where

$$S_{\kappa}^X(q^2) = X_{\kappa} r(y), \quad y = q^2/\kappa^2, \quad (21)$$

and

$$\kappa \partial_{\kappa} S_{\kappa}^X(y) = -X_{\kappa} (\eta_{\kappa}^X r(y) + 2y \partial_y r(y)). \quad (22)$$

and we use the notation

$$X \in \{D, \parallel, \perp\}, \quad X_{\kappa} \in \{D_{\kappa}, \nu_{\kappa}^{\parallel}, \nu_{\kappa}^{\perp}\}, \quad \eta_{\kappa}^X \in \{\eta_{\kappa}^D, \eta_{\kappa}^{\parallel}, \eta_{\kappa}^{\perp}\}. \quad (23)$$

The running coefficients X_{κ} and anomalous dimensions η_{κ}^X will be defined later in Eq. (26). Within the NLO approximation, the remaining n -point functions all vanish, except

$$\Gamma_{\kappa}^{(2,1)}(\omega_1, \omega_2; \vec{p}_{\parallel 1}, \vec{p}_{\parallel 2}, \vec{p}_{\perp 1}, \vec{p}_{\perp 2}) = (\lambda_{\parallel} \vec{p}_{\parallel 1} \cdot \vec{p}_{\parallel 2} + \lambda_{\perp} \vec{p}_{\perp 1} \cdot \vec{p}_{\perp 2}) f_{\kappa}^{\lambda}(|\vec{p}_{\parallel 1} + \vec{p}_{\parallel 2}|, |\vec{p}_{\perp 1} + \vec{p}_{\perp 2}|). \quad (24)$$

D. Dimensionless flowing functions

To analyze the fixed-point properties of the flow equations, dimensionless and renormalized quantities (indicated by a hat) are introduced. Momentum and frequency are measured in units of the running cutoff $\kappa_{\parallel} \equiv \kappa$

$$\hat{p}_{\parallel} = p_{\parallel}/\kappa, \quad \hat{p}_{\perp} = p_{\perp}/(\gamma_{\kappa}^{1/2} \kappa), \quad \hat{\omega} = \omega/(\nu_{\kappa}^{\parallel} \kappa^2), \quad (25)$$

and we define three running coefficients $\{D_{\kappa}, \nu_{\kappa}^{\parallel}, \nu_{\kappa}^{\perp}\}$ and the related anomalous dimensions η_{κ}^X via

$$\eta_{\kappa}^D = -\kappa \partial_{\kappa} \ln D_{\kappa}, \quad \eta_{\kappa}^{\parallel} = -\kappa \partial_{\kappa} \ln \nu_{\kappa}^{\parallel}, \quad \eta_{\kappa}^{\perp} = -\kappa \partial_{\kappa} \ln \nu_{\kappa}^{\perp}. \quad (26)$$

At the initial cutoff scale $\kappa \equiv \Lambda$ the running coefficients are equal to unity: $D_{\Lambda} = \nu_{\Lambda}^{\parallel/\perp} = 1$. Due to the Galilean symmetry Eq. (4a) both coefficients $\lambda_{\parallel/\perp}$ are not renormalized and thus no additional running couplings are needed for them. We define the anisotropy ξ , dynamical z and roughness χ exponents as

$$x_{\perp} \sim x_{\parallel}^{\xi}, \quad t \sim x_{\parallel}^z, \quad h \sim x_{\parallel}^{\chi}. \quad (27)$$

With the field dimensions $[h(\mathbf{x})] = (\kappa^{d-2} D_{\kappa} \gamma_{\kappa}^{d_{\perp}/2} / \nu_{\kappa}^{\parallel})^{1/2}$ and $[\tilde{h}(\mathbf{x})] = (\kappa^{d+2} \nu_{\kappa}^{\parallel} \gamma_{\kappa}^{d_{\perp}/2} / D_{\kappa})^{1/2}$ and the rescaling Eq. (25), the physical critical exponents can be deduced from the anomalous dimensions at a fixed point (indexed by a star) via

$$\xi = 1 - (\eta_{*}^{\parallel} - \eta_{*}^{\perp})/2, \quad (28a)$$

$$z = 2 - \eta_{*}^{\parallel}, \quad (28b)$$

$$\chi = (2 - d + \eta_{*}^D - \eta_{*}^{\parallel} + d_{\perp}/2(\eta_{*}^{\parallel} - \eta_{*}^{\perp}))/2. \quad (28c)$$

Expressed in terms of dimensionless quantities, the AKPZ flow equations depend on the two dimensionless couplings

$$\hat{g}_{\kappa}^{\parallel} = g_b^{\parallel} \kappa^{d-2} \left(\frac{D_{\kappa} \gamma_{\kappa}^{d_{\perp}/2}}{\nu_{\parallel \kappa}^3} \right), \quad (29a)$$

$$\hat{g}_{\kappa}^{\perp} = \hat{g}_{\kappa}^{\parallel} \gamma_{\kappa}^2 \frac{g_b^{\perp}}{g_b^{\parallel}}, \quad (29b)$$

where the bare couplings are defined in Eq. (A6). We will not study the flow in terms of the nonlinear couplings $\hat{g}_{\kappa}^{\parallel}$ and \hat{g}_{κ}^{\perp} directly, but rather in terms of $\hat{g}_{\kappa}^{\parallel} \equiv \hat{g}_{\kappa}$ and the anisotropy ratio γ_{κ} . The flows of the coupling and of the anisotropy are

$$\partial_s \hat{g}_{\kappa} = \hat{g}_{\kappa} (d - 2 - \eta_{\kappa}^D + 3\eta_{\kappa}^{\parallel} - (d_{\perp}/2)(\eta_{\kappa}^{\parallel} - \eta_{\kappa}^{\perp})), \quad (30a)$$

$$\partial_s \gamma_{\kappa} = -\gamma_{\kappa} (\eta_{\kappa}^{\parallel} - \eta_{\kappa}^{\perp}), \quad (30b)$$

where $s = \ln(\Lambda/\kappa)$ with $\partial_s \equiv \kappa \partial_{\kappa}$ is the so-called RG ‘‘time’’.

Further, dimensionless running functions with two momentum arguments are defined by

$$\hat{f}_{\kappa}^X(\hat{p}_{\parallel}, \hat{p}_{\perp}) = f_{\kappa}^X(p_{\parallel}, p_{\perp})/X_{\kappa}, \quad (31)$$

for $X \in \{D, \nu, \lambda\}$ and $X_\kappa \in \{D_\kappa, \nu_\kappa^\parallel, 1\}$. Their flows are given by

$$\begin{aligned} \partial_s \hat{f}_\kappa^X(\hat{p}_\parallel, \hat{p}_\perp) &= \eta_\kappa^X \hat{f}_\kappa^X(\hat{p}_\parallel, \hat{p}_\perp) + \hat{p}_\parallel \partial_{\hat{p}_\parallel} \hat{f}_\kappa^X(\hat{p}_\parallel, \hat{p}_\perp) \\ &+ (1 - \eta_\kappa^\parallel/2 + \eta_\kappa^\perp/2) \hat{p}_\perp \partial_{\hat{p}_\perp} \hat{f}_\kappa^X(\hat{p}_\parallel, \hat{p}_\perp) + \hat{I}_\kappa^X(\hat{p}_\parallel, \hat{p}_\perp), \end{aligned} \quad (32)$$

with $\eta_\kappa^X \in \{\eta_\kappa^D, \eta_\kappa^\parallel, 0\}$, and $\hat{I}_\kappa^X(\hat{p}_\parallel, \hat{p}_\perp)$ are the loop integrals

$$\hat{I}_\kappa^X(\hat{p}_\parallel, \hat{p}_\perp) = (\kappa \partial_\kappa f_\kappa^X(p_\parallel, p_\perp))/X_\kappa. \quad (33)$$

At the origin, the scale dependent functions are normalized such that $\hat{f}_\kappa^X(0, 0) = 1$.

Finally, we have to calculate the flow of the anomalous dimensions from the ansatz for Γ_κ . We deduce from the 2-point functions in Eqs. (15) that the running coefficients can be expressed as

$$\nu_\kappa^\parallel = \lim_{\omega \rightarrow 0, \vec{p}_\parallel \rightarrow 0} \left(\lim_{\vec{p}_\perp \rightarrow 0} \Gamma^{(1,1)}(\omega, \vec{p}_\parallel, \vec{p}_\perp) / \vec{p}_\parallel^2 \right), \quad (34a)$$

$$\nu_\kappa^\perp = \lim_{\omega \rightarrow 0, \vec{p}_\perp \rightarrow 0} \left(\lim_{\vec{p}_\parallel \rightarrow 0} \Gamma^{(1,1)}(\omega, \vec{p}_\parallel, \vec{p}_\perp) / \vec{p}_\perp^2 \right), \quad (34b)$$

$$D_\kappa = - \lim_{\omega \rightarrow 0, \vec{p}_\perp \rightarrow 0, \vec{p}_\parallel \rightarrow 0} \Gamma^{(0,2)}(\omega, \vec{p}_\parallel, \vec{p}_\perp) / 2. \quad (34c)$$

Note the ordering of the limits for the two momenta to obtain the parallel and perpendicular components. From Eq. (33), we further define loop integrals with zero external arguments

$$\hat{I}_\kappa^\parallel = \lim_{\omega \rightarrow 0, \vec{p}_\parallel \rightarrow 0} \left(\lim_{\vec{p}_\perp \rightarrow 0} \kappa \partial_\kappa \Gamma^{(1,1)}(\omega, \vec{p}_\parallel, \vec{p}_\perp) / (\nu_\kappa^\parallel \vec{p}_\parallel^2) \right), \quad (35a)$$

$$\hat{I}_\kappa^\perp = \lim_{\omega \rightarrow 0, \vec{p}_\perp \rightarrow 0} \left(\lim_{\vec{p}_\parallel \rightarrow 0} \kappa \partial_\kappa \Gamma^{(1,1)}(\omega, \vec{p}_\parallel, \vec{p}_\perp) / (\nu_\kappa^\perp \vec{p}_\perp^2) \right), \quad (35b)$$

$$\hat{I}_\kappa^D = - \lim_{\omega \rightarrow 0, \vec{p}_\perp \rightarrow 0, \vec{p}_\parallel \rightarrow 0} \kappa \partial_\kappa \Gamma^{(0,2)}(\omega, \vec{p}_\parallel, \vec{p}_\perp) / (2D_\kappa). \quad (35c)$$

Therefore, from the definition of the anomalous dimensions Eq. (26) and Eqs. (34, 35)

$$0 = \eta_\kappa^X + \hat{I}_\kappa^X \quad (36)$$

follows, where $X \in \{D, \parallel, \perp\}$. Due to the regulator each integral \hat{I}_κ^X itself depends linearly on η_κ^X and can be written in the form

$$\hat{I}_\kappa^X = \hat{I}_\kappa^{XD} \eta_\kappa^D + \hat{I}_\kappa^{X\parallel} \eta_\kappa^\parallel + \hat{I}_\kappa^{X\perp} \eta_\kappa^\perp + \hat{I}_\kappa^{X0}. \quad (37)$$

Eqs. (36) and (37) thus form a linear set of equations that can be solved for the exponents. Explicit expressions for the integrals \hat{I}_κ^{XY} with $X, Y \in \{D, \parallel, \perp\}$ are given in Eqs. (A7, A8) of the appendix.

The NLO approximation [47] noticeably reduces the complexity of the flow equations but the loop-integrals

in Eqs. (33) are still four-dimensional integrals and numerically cumbersome. However, for a qualitative picture of the phase diagram it is sufficient to consider only the flow of the scale dependent couplings and to set all flowing functions to one:

$$\hat{f}_\kappa^X(\hat{p}_\parallel, \hat{p}_\perp) \rightarrow \hat{f}_\kappa^X(0, 0) \equiv 1. \quad (38)$$

This approximation is usually referred to as Local Potential Approximation prime (LPA') [49]. For the isotropic KPZ equation the roughness exponent χ is overestimated at the LPA' level but the qualitative behavior and the correct strong-coupling physics is already obtained. In addition, the LPA' allows to study analytically the weak-coupling limit of the flow and we recover the results of TF in that limit, see appendix A. Only in order to test the robustness of the various features of the phase diagram obtained in the LPA' approximation, we will resort to the NLO approximation. A similar strategy, with both LPA' and NLO, was adopted to study the long-range KPZ equation in a previous study [48]. Hence, in the following, the LPA' results are presented, except when they disagree with the NLO ones, which will be indicated.

E. Numerical implementation

In the LPA' approximation the two flow equations (30) for the couplings, and in addition the three flow equations (32) for the running functions at NLO, are solved numerically by explicit Euler time stepping. Stable fixed point solutions are typically found for RG “times” $s \leq -10$. The flowing functions $\hat{f}_\kappa^X(\hat{p}_\parallel, \hat{p}_\perp)$ are discretized on rectangular and equidistant $\hat{p}_\parallel \times \hat{p}_\perp$ grids. Between the grid-points, they are interpolated by bi-cubic splines. Numerical integrations over the two radial momentum components and over the two angles are performed by Gauss-Legendre quadrature. In the LPA' approximation, the two-dimensional radial integrals for \hat{I}_κ^X Eqs. (A7) are reduced to one-dimensional integrals by Eq. (A9). We initialize all flowing functions at $\hat{f}_\kappa^X(\hat{p}_\parallel, \hat{p}_\perp) = 1$.

III. RESULTS

A. NPRG fixed point solutions

We present in the following the various fixed point solutions that we find within our NPRG approach. As can be inferred from the β functions (30), all the set ($\hat{g} = 0, \gamma$) is a continuous line of fixed points. Within them, there are particular points where the flow along the γ direction is vanishing even for a nonzero but small coupling \hat{g} . We will refer to these points as Edwards Wilkinson like fixed points. Quite generally, for all EW like solutions where the coupling $\hat{g}_\kappa \rightarrow \hat{g}_* = 0$, namely EW, EWA and EWU, we find the same results as TF with the perturbative approach. In particular, we recover the same

stability conditions as TF and find the EW exponents $\chi_{\text{EW}} = (2-d)/2$ and $z_{\text{EW}} = 2$ since $\eta_*^D = \eta_*^{\parallel} = \eta_*^{\perp} = 0$ for all three weak-coupling solutions. It is further clear that the isotropic fixed point solutions (with $\gamma_* = 1$) of the AKPZ equation are also solutions of the KPZ equation. These solutions are therefore independent of the splitting into the sector dimensions d_{\parallel} and d_{\perp} , and depend only on the total dimension d .

Finally, let us define for convenience the rescaled coupling constant $\hat{g}' = v_d \hat{g}/4$ with $v_d^{-1} = 2^{d-1} \pi^{d/2} \Gamma(d/2)$, that will be used for the graphical representation of the RG flows throughout this article.

1. Isotropic Edwards-Wilkinson fixed point (EW)

The isotropic EW fixed point corresponds to $(\hat{g}_*, \gamma_*) = (0, 1)$. This fixed point is repulsive (resp. attractive) in the \hat{g} direction for $d \leq 2$ (resp. $d > 2$). In the direction of the anisotropy γ , the EW fixed point is attractive for $d < \sqrt{8}$ and repulsive for $d > \sqrt{8}$.

2. Anisotropic Edwards-Wilkinson fixed point (EWA)

The anisotropic EWA fixed point is located at $(\hat{g}_*, \gamma_*) = (0, (4-d_{\parallel}d)/(dd_{\perp}-4))$. It is repulsive (resp. attractive) in the \hat{g} direction for $d < 2$ (resp. $d > 2$). At exactly $d = 2$, EWA is repulsive (resp. attractive) for $d_{\parallel} \geq 1 + 1/\sqrt{5}$ (resp. $d_{\parallel} < 1 + 1/\sqrt{5}$). In the direction of the anisotropy γ , the EWA fixed point is attractive for $d < -\Delta/2 + \sqrt{(\Delta/2)^2 + 8}$ and $\sqrt{8} < d < \Delta/2 + \sqrt{(\Delta/2)^2 + 8}$ and repulsive for $-\Delta/2 + \sqrt{(\Delta/2)^2 + 8} < d < \sqrt{8}$ and $d > \Delta/2 + \sqrt{(\Delta/2)^2 + 8}$ with $\Delta = d_{\parallel} - d_{\perp}$.

3. Uniaxial Edwards-Wilkinson fixed point (EWU)

The uniaxial EWU fixed point at $(\hat{g}_*, \gamma_*) = (0, 0)$ corresponds to the situation when λ_{\perp} is zero. It is repulsive (resp. attractive) in the \hat{g} direction for $d < 2$ (resp. $d > 2$). Exactly at $d = 2$, EWU is repulsive (resp. attractive) in the \hat{g} direction for $d_{\parallel} \geq -1 + \sqrt{5}$ (resp. $d_{\parallel} < -1 + \sqrt{5}$). In the direction of the anisotropy γ , the EWU fixed point is repulsive for $d < -\Delta/2 + \sqrt{(\Delta/2)^2 + 8}$ and attractive for larger values of d . A second EWU_{∞} fixed point at $(0, \infty)$ corresponds to the reverse situation when λ_{\parallel} is equal to zero.

4. Isotropic Transition fixed point (T)

The transition fixed point T is located at $\gamma_* = 1$ and $\hat{g}_* > 0$ and exists for $d > 2$. It is always repulsive in the \hat{g} direction. In the direction of the anisotropy γ it is stable against anisotropic perturbations for smaller d but becomes unstable for larger values of d when the

TA fixed point crosses it. The exponents are exactly known: $\chi_T = 0$ and $z_T = 2$ in all dimensions. Within our approximation scheme, they are slightly underestimated (e.g. in $d = 3$ we find $\chi_T = -0.08$ (resp. -0.12) in NLO (resp. LPA') approximation).

5. Anisotropic Transition fixed point (TA)

The anisotropic transition fixed point is unstable and located at $\hat{g}_* > 0$. It is found for $d > 2$ and when the difference between the sector dimensions is sufficiently large so that the anisotropic fixed point A is present. TA is always repulsive in the \hat{g} direction. In the direction of the anisotropy, TA is attractive for smaller values of d when the TA fixed point is in the $\gamma < 0$ quadrant but becomes unstable when it crosses the TU fixed point and moves into the $0 < \gamma_* < 1$ quadrant. TA reverts to attractive when it crosses the T fixed point at $\gamma_* = 1$ and turns into the $\gamma_* > 1$ quadrant. For $d > 2$ and small differences between the sector dimensions, TA merges with the TU fixed point at $\gamma_* = 0$, see Fig. 5.

6. Uniaxial Transition fixed point (TU)

The uniaxial transition fixed point is unstable and located at $\hat{g}_* > 0$ and $\gamma_* = 0$. It is found for $d > 2$ when the difference between the sector dimensions is sufficiently large so that the uniaxial U fixed point is present. TU is always unstable in the \hat{g} direction. In the direction of the anisotropy, TU is attractive for smaller values of d when the TA fixed point is in the $\gamma < 0$ quadrant but becomes unstable when TA crosses it to move into the $\gamma > 0$ quadrant. For $d > 2$ and a decreasing difference between the sector dimensions, TU merges with the TA and the A fixed point before it annihilates with U, see Fig. 5.

7. Isotropic Strong coupling fixed point (SC)

The strong coupling fixed point SC is located at $\gamma_* = 1$ and $\hat{g}_* > 0$ and describes the isotropic rough phase of the KPZ equation. Within the NLO approximation, the associated exponents are in good agreement with the numerical ones in $d = 2$ and $d = 3$ [45–47]. The quality of the NLO approximation in the isotropic case deteriorates with increasing dimension and it does not yield reliable quantitative results above typically $d \simeq 3.5$. In all dimensions at the LPA', and in all dimensions $d \lesssim 3.5$ at the NLO approximation, we find the SR fixed point to be locally stable and fully attractive.

8. Anisotropic fixed point (A)

The anisotropic fixed point A is located at $\gamma_* < 0$ and $\hat{g}_* > 0$. It is fully attractive for $d < 2$ and for $d = 2$ when $d_{\parallel} > 1 + 1/\sqrt{5}$. For $d = 2$ and $d_{\parallel} = 1 + 1/\sqrt{5}$ it coincides with the EWA fixed point and moves to the negative quadrant for smaller values of d_{\parallel} . For $d > 2$, A is found for a large enough splitting between the sector dimensions. In that case it is also fully attractive but the dominant exponents around A may become complex. To the best of our knowledge, this fixed point was not found yet and may correspond to a new rough anisotropic phase. Unfortunately, we find it only at non-integer dimensions. In consequence, its physical role is not clear.

9. Uniaxial fixed point (U)

The uniaxial strong-coupling fixed point U is present for $d < 2$ and in $d = 2$ when $d_{\parallel} > -1 + \sqrt{5}$. It is attractive in the direction \hat{g} , but repulsive in the anisotropy direction γ . At $d = 2$ and $d_{\parallel} = -1 + \sqrt{5}$ it crosses the EWU fixed point and moves to the unphysical quadrant for smaller values of d_{\parallel} . For $d > 2$ and a decreasing difference between both sector dimensions, U annihilates with the transition fixed point TU.

B. Phase diagram

After the characterization of the various fixed point solutions, let us discuss the phase diagram of the AKPZ equation in the (\hat{g}', γ) plane. For the EW like weak-coupling fixed points we recover the same stability conditions as TF in Ref. [29]. That is, the stability of the weak-coupling fixed points against anisotropic perturbations is changed by the EWA fixed point, which moves along the $(\hat{g} = 0, \gamma)$ line as a function of d_{\parallel} and d_{\perp} . When EWA crosses the other fixed points EWU, EW and EWU $_{\infty}$, they interchange their stability. The sector dimensions d_{\parallel} and d_{\perp} that we find at which EWA crosses the other EW like fixed points agree with those found by TF. Apart from this vertical stability condition reflecting the effect of anisotropic perturbations, horizontal stability changes also occur to the EW like fixed points. This effect is already visible at the perturbative level, but requires nonperturbative methods to be thoroughly studied, since the crossing fixed points can become strong coupling in certain parameter regimes as detailed in the appendix D. This analysis goes beyond the one of TF. In the following we will show how the inclusion of the strong-coupling part changes qualitatively our understanding of the phase diagram.

1. The case $d < 2$

First, the situation d below 2 is depicted in Fig. 1. All EW like fixed points are unstable in the horizontal direction and three additional fixed points are found; one unstable U and two locally stable SC and A fixed points. When both nonlinear couplings have the same sign, which corresponds to the flow in the positive γ quadrant of Fig. 1, the flow is always attracted by the SC fixed point and the well known isotropic KPZ rough phase is found. On the other hand, if the couplings have opposite signs, which corresponds to the flow in the negative γ quadrant, the flow is always driven towards the A fixed point.

2. The case $d = 2$

Second, exactly at $d = 2$ the horizontal stability of the EW like fixed points depend on the splitting in the sector dimensions. The RG flow for an increasing difference between d_{\parallel} and d_{\perp} is depicted in Fig. 2. In this figure, the panel (a) corresponds to Wolf's result [8] with $d_{\parallel} = d_{\perp} = 1$. That is, the EW fixed point is repulsive and EWU and EWA are both attractive in the horizontal direction. When both nonlinear couplings have the same sign, the flow is always attracted by the SC fixed point. On the other hand, if the couplings have opposite signs, the flow is always driven towards the weak-coupling EWA fixed point. The situation changes when the difference between the sector dimensions increases. For $d_{\parallel} > -1 + \sqrt{5}$, first EWU becomes repulsive in the horizontal direction, see Fig. 2 (b). This stability change is caused by the U fixed point, which crosses EWU at $d_{\parallel} = -1 + \sqrt{5}$ and enters the physical quadrant. Since U is unstable the flow is still attracted towards SC or EWA if $\gamma \neq 0$. However, if the difference between the two sector dimensions is further increased above $d_{\parallel} > 1 + 1/\sqrt{5}$ also EWA is crossed by A and turns repulsive in the horizontal direction, see Fig. 2 (c). For positive γ the SC fixed point continues to be the only attractive fixed point, but in the negative γ quadrant, the flow is driven towards A, similarly to the situation in $d < 2$.

3. The case $2 < d \leq 3$

For $d > 2$ all EW like fixed points become attractive in the horizontal direction. In the cases where in $d = 2$ an EW like fixed point is already attractive in the horizontal direction, it remains so. In the cases where it is not in $d = 2$, a transition fixed point crosses it as shown in Fig. 3 and the EW like fixed point becomes stable in the horizontal direction.

When d increases the ordering of the transition fixed points T, TU and TA may be different from the ordering of the EW like fixed points (see Figs. 3 and 4). For d larger than 2 and arbitrary splitting in the two sectors, we find the flow in certain cases to be more complex.

For example in $d = 3$ we observe the flows shown in Fig. 5. One sees that for certain values of the splitting the dominant exponents around the A fixed point are complex. This gives a flow in form of spirals. Similar situations, with fixed points having a spiral flow were already observed for example in Ref. [63]. Unfortunately, we do not find the A fixed point at $d = 3$ for integer values of the sector dimensions. If such a behavior had been present, it would imply a new anisotropic universality class in physical situations. In the positive γ region we did not find any case in which the isotropic SC fixed point becomes locally unstable. For the physically relevant case where both sector dimensions take integer values ($d_{\parallel} = 2, d_{\perp} = 1$) we find the flow shown in Fig. 5(d). The flow at the NLO approximation is slightly different as shown in Fig. 6. However, in both approximations there is a critical coupling value \hat{g}_c in the positive γ quadrant which is given by the separatrix (highlighted in blue) that goes through T. If the coupling is below this critical value, the flow renormalizes the coupling to zero and EW physics is obtained. For a sufficiently large coupling $\hat{g} > \hat{g}_c$ the flow is attracted towards the SC fixed point, yielding the rough isotropic phase.

4. The case $d > 3$

As already pointed out, the NLO approximation turns out to become unreliable in the isotropic strong coupling regime for dimensions $d \gtrsim 3.5$ [45, 47, 48]. In large dimensions one typically do find the strong coupling fixed point but the associated critical exponents largely depend on the regulator. However, the quality of the NLO approximation around the anisotropic or the uniaxial fixed point is *a priori* not known. In the physically relevant cases $d_{\parallel} = d_{\perp} = 2$ and $d_{\parallel} = 3$ with $d_{\perp} = 1$ we find the isotropic strong coupling fixed point always locally stable, both within the LPA' and the NLO approximations [64]. The flow is qualitatively similar to Fig. 5 (e) when $d_{\parallel} = d_{\perp} = 2$, whereas it resembles Fig. 4 when $d_{\parallel} = 3$ and $d_{\perp} = 1$ [65]. In contrast to the former case in $d = 3$, we find the A fixed point for the integer splitting $d_{\parallel} = 3$ and $d_{\perp} = 1$ at LPA', but it is not present at NLO. This indicates that the LPA' (or even NLO) approximation may be unreliable in this regime of the flow.

C. On the stability of the rough isotropic phase

In the previous section we stressed that the strong coupling behavior in the positive γ quadrant is always driven by a unique and locally fully attractive SC fixed point. For non-integer dimensions we find other fixed points A and U, but they stay in the negative γ quadrant (resp. at $\gamma = 0$). As already mentioned, we do not observe that these fixed points enter the positive γ quadrant. Hence, they do not cross the SC fixed point and leave its stability unchanged. Physically, this implies that the isotropic

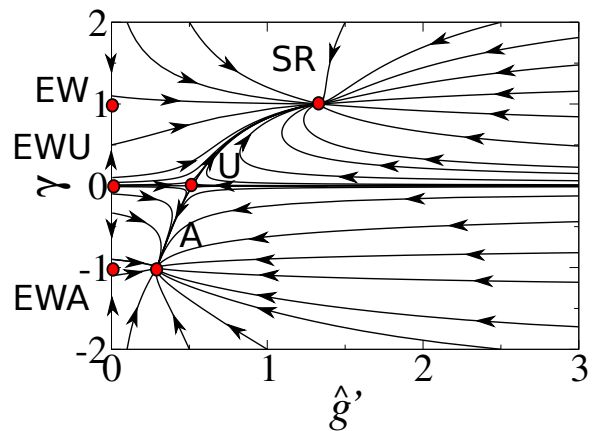


FIG. 1. (Color online) Typical RG trajectories in the $(\hat{g}', \tilde{\gamma})$ plane for $d < 2$ (here $d_{\parallel} = d_{\perp} = 0.8$). All weak coupling fixed points EW (with $\gamma_* = 1$), EWU (with $\gamma_* = 0$) and EWA (with $\gamma_* = (4 - d_{\parallel}d)/(dd_{\perp} - 4)$) are unstable and we find two locally stable strong-coupling fixed points SC (with $\gamma_* = 1$) and A (with $\gamma_* < 0$). Moreover, there is another U fixed point with $\gamma_* = 0$.

rough phase is locally stable against anisotropic perturbations even for arbitrary non-integer sector dimensions. Our work generalizes the one of TF [29] since we are able to study the strong coupling regime. In agreement with TF we find that the isotropic KPZ equation may become unstable against anisotropic perturbations in the weak-coupling regime. However, our results indicate that it is not possible to make a naïve extrapolation from the perturbative results to the strong coupling regime in order to predict the stability of the SC phase. In contrast to the weak-coupling regime the isotropic strong coupling fixed point SC remains always locally stable.

IV. CONCLUSION

In this manuscript, we have presented a NPRG ansatz to study the AKPZ equation. We have derived the associated flow equations and solved them numerically to study the RG flow and their fixed point solutions. Two different approximations were applied throughout this study, the simpler LPA' approximation to obtain the qualitative features of the phase diagram and the more accurate NLO approximation in order to check our findings.

At weak coupling the LPA' approximation leads to the same equations (and stability conditions) as the perturbative ones in the study by TF, but moreover, with the NPRG ansatz we are able to study the strong coupling regime. We find that the isotropic rough KPZ phase is always locally stable against anisotropic perturbations. The AKPZ equation provides no hint for the existence of an upper critical dimension of the strong-coupling phase (similarly to the conclusion drawn from the analysis of the KPZ equation with long-range noise [48]). In fact, if both nonlinear couplings have the same sign, the be-

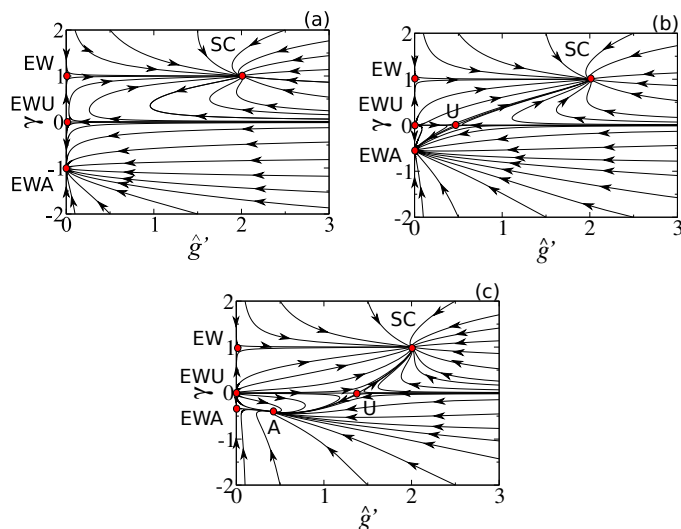


FIG. 2. (Color online) RG trajectories in the $(\hat{g}', \gamma_{\kappa})$ plane at $d = 2$ with an increasing difference between the sector dimensions (from up do down). Panel (a) represents a typical flow for $d_{\parallel} < -1 + \sqrt{5}$ (here $d_{\parallel} = d_{\perp} = 1$, which corresponds to Wolf's result [8]). Both the anisotropic fixed point EWA and the isotropic SC fixed point are fully attractive. The uniaxial fixed point EWU is attractive in the \hat{g} direction but unstable in the anisotropy direction. Panel (b): Typical flow for $-1 + \sqrt{5} < d_{\parallel} < 1 + 1/\sqrt{5}$ (here $d_{\parallel} = 1.3$ and $d_{\perp} = 0.7$). EWU is now repulsive in the \hat{g} direction. Panel (c): Typical flow for $d_{\parallel} > 1 + 1/\sqrt{5}$ (here $d_{\parallel} = 1.5$ and $d_{\perp} = 0.5$). EWA becomes repulsive in the \hat{g} direction because the anisotropic fixed point A crosses it. Note that in all cases the isotropic fixed point SC is not affected by the weak coupling stability changes and is always fully attractive.

havior of the AKPZ equation resembles much that of the standard KPZ equation and the critical exponents χ and z depend only on the total spatial dimension d but not on the splitting in the two sector dimensions. That is, for $d \leq 2$ the flow is always driven towards the isotropic rough strong coupling fixed point. For $d > 2$ there is a critical coupling \hat{g}_c below which the flow renormalizes the coupling to zero and EW physics is obtained. In contrast, for sufficiently large coupling $\hat{g} > \hat{g}_c$ the flow is attracted towards the SC fixed point, describing the rough isotropic phase. The anisotropy plays no role in that case.

However, if the nonlinearities have different signs, the anisotropy becomes relevant. The case $d_{\parallel} = d_{\perp} = 1$, initially studied by Wolf who found only weak coupling behaviors, turns out to be only a special case, as already pointed out by TF. In the general situation, we find a new locally attractive anisotropic strong-coupling fixed point, that could had corresponded to a new universality class. However, it is only present for certain non-integer values of d_{\parallel} and d_{\perp} , and does not exist at integer sector dimensions.

We hope that our results might have some relevance for the physics of cold atoms, considering the recently established connection with an anisotropic and periodic

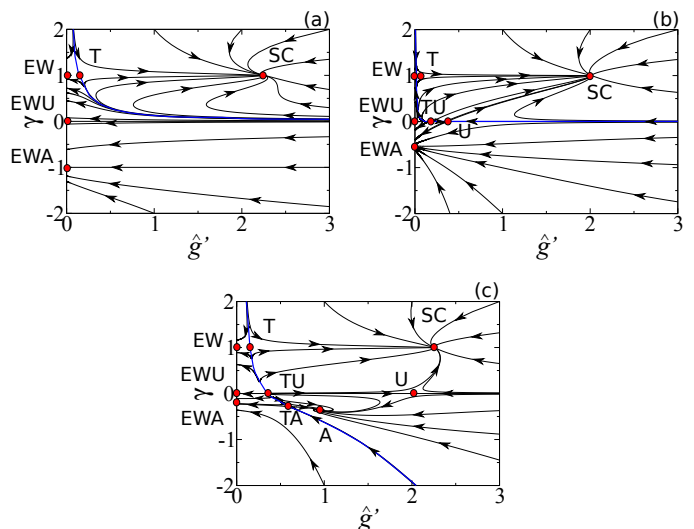


FIG. 3. (Color online) RG trajectories in the $(\hat{g}', \gamma_{\kappa})$ plane for $d > 2$ but with small $d - 2$. The difference between the sector dimensions increases along the panels. Panel (a): Typical flow for $d > 2$ with small $d - 2$ and $d_{\parallel} \lesssim 1.2$ (here $d_{\parallel} = d_{\perp} = 1.1$). EW is attractive in the horizontal direction and one unstable transition fixed point T ($\gamma_* = 1$) is present. Panel (b): Typical flow for $d > 2$ with small $d - 2$ and $1.2 \lesssim d_{\parallel} \lesssim 1.4$ (here $d_{\parallel} = 1.31$ and $d_{\perp} = 0.702$). EW and EWU are attractive in the horizontal direction and two unstable transition fixed points T and TU ($\gamma_* = 0$) are present. Panel (c): Typical flow for $d > 2$ with small $d - 2$ and $1.4 \lesssim d_{\parallel}$ (here $d_{\parallel} = 1.7$ and $d_{\perp} = 0.5$). EW, EWU and EWA are attractive in the horizontal direction and three unstable transition fixed points T, TU and TA ($\gamma_* < 0$) are present.

variant of the KPZ equation [9, 10]. The AKPZ equation readily incorporates the effect of anisotropy but ignores that of periodicity. At the current stage it seems however not possible to predict the importance of this missing ingredient and how it might change the results if present. This work is left for further studies.

V. ACKNOWLEDGMENTS

LC and TK thank the Universidad de la República, NW the LPMCM and TK the Goethe Universität Frankfurt and the Group of P. Kopietz for hospitality. This work has received financial support from PEDECIBA program, the ECOS France-Uruguay collaboration program and TK acknowledges financial support from the IIP in Natal. Numerical calculations were performed on the Computer System of High Performance (IIP and UFRN, Natal) and on HOUSEWIVES (Goethe Universität, Frankfurt). The authors would also like to thank B. Delamotte for stimulating discussions.

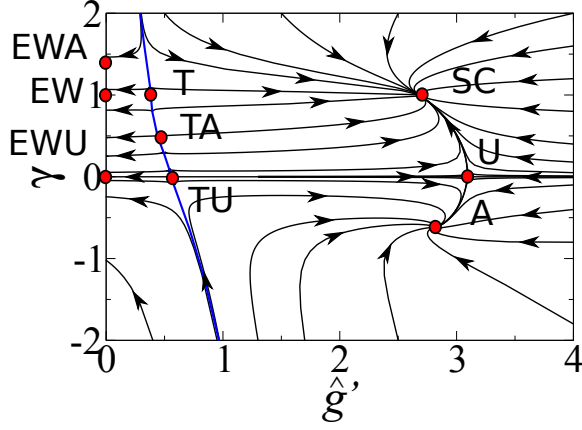


FIG. 4. (Color online) RG trajectories in the $(\hat{g}'_\kappa, \gamma_\kappa)$ plane. Typical flow for d approaching 3 with $d_\perp \sim 0.5$ (here $d_\parallel = 2.5$ and $d_\perp = 0.5$). The unstable transition fixed points T ($\gamma_* = 1$), TA ($0 < \gamma_* < 1$) and TU ($\gamma_* = 0$) are present. The ordering of the three transition fixed points along the γ axis is no longer the same as the one of the weak coupling solutions (EWA, EW and EWU). It is useful to compare with Fig. 3.

APPENDIX A: PERTURBATIVE ANALYSIS IN THE WEAK-COUPLING LIMIT

In the limit $\hat{g}_\kappa \rightarrow 0$, the anomalous dimensions simplify to

$$\eta_\kappa^D = -\hat{I}_\kappa^{D0}, \quad \eta_\kappa^\parallel = -\hat{I}_\kappa^{\parallel 0}, \quad \eta_\kappa^\perp = -\hat{I}_\kappa^{\perp 0}. \quad (\text{A1})$$

As emphasized in previous studies [48], the NLO approximation reduces to the LPA' approximation in that limit because the difference of the flowing functions f^X to one is already of order \hat{g} . We can therefore take the limit of small coupling directly in the LPA' approximation Eq. (38) and calculate explicitly the loop integrals Eqs. (A7) to obtain

$$\eta_\kappa^D = \hat{g}_\kappa [d_\parallel(d_\parallel + 2) + d_\perp(d_\perp + 2)\gamma_\kappa^2 + 2d_\parallel d_\perp \gamma_\kappa] A(d), \quad (\text{A2a})$$

$$\eta_\kappa^\parallel = -\hat{g}_\kappa [d(d_\parallel + d_\perp \gamma_\kappa) - 4] A(d), \quad (\text{A2b})$$

$$\eta_\kappa^\perp = -\hat{g}_\kappa \gamma_\kappa [d(d_\parallel + d_\perp \gamma_\kappa) - 4\gamma_\kappa] A(d). \quad (\text{A2c})$$

These expressions are, up to the inverse sign convention and the extra factor

$$A(d) = -\frac{v_d}{2d(d+2)} \int_0^\infty d\hat{q} \hat{q}^{d-1} \frac{\partial_{\hat{q}^2} r(\hat{q}^2)}{(1+r(\hat{q}^2))^2}, \quad (\text{A3})$$

similar to the one-loop results of TF [29]. The integral $A(d)$ is a positive constant which depends only on the dimension and on the cutoff function. Note that for the special value $d = 2$ this integral is independent of the regulator and we find $A(2) = 1/(64\pi)$. The factor $A(d)$ can further be absorbed by a simple redefinition of \hat{g}_κ . For all EW like fixed points we therefore recover exactly the same stability conditions as TF.

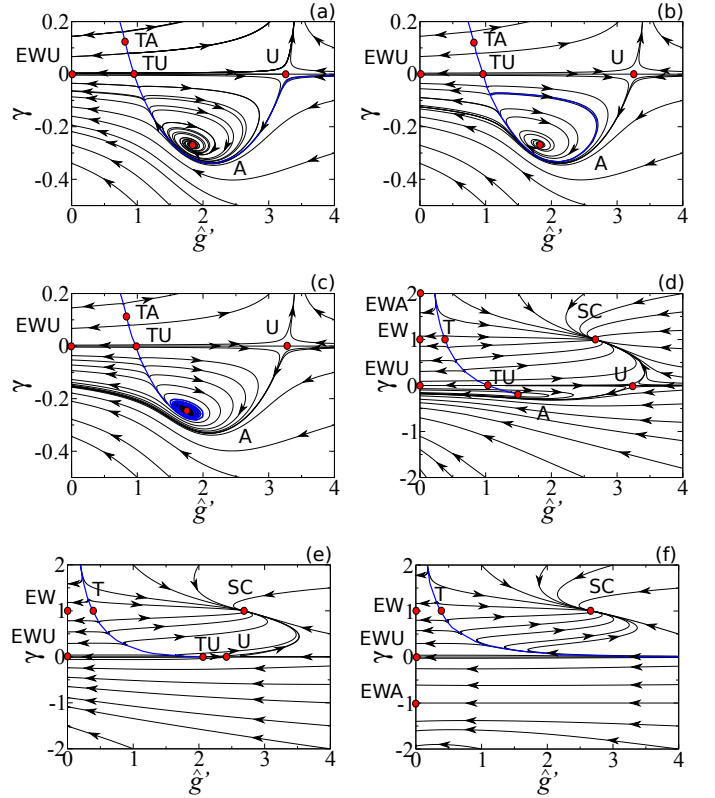


FIG. 5. (Color online) RG trajectories in the $(\hat{g}_\kappa, \gamma_\kappa)$ plane for $d = 3$ and a decreasing difference between both sector dimensions (from up to down). Panel (a): The fixed point A is enclosed by the $\gamma = 0$ axis and the separatrix (highlighted in blue) and shows a spiral flow. (here $d_\parallel = 2.04855$ and $d_\perp = 0.95145$). Panel (b): The separatrix has formed a closed loop around A. Inside this loop, the flow is directed towards A, outside and for $\gamma < 0$ the couplings always flow to the weak coupling regime. (here $d_\parallel = 2.047$ and $d_\perp = 0.953$). Panel (c): The enclosed area around A decreases in size. (here $d_\parallel = 2.035$ and $d_\perp = 0.965$). Panel (d): The size of the attractive zone around A shrank down to zero. The TA fixed point has approached TU at $\gamma = 0$ and merges with it. (here $d_\parallel = 2$ and $d_\perp = 1$). Panel (e): The endpoint of the separatrix where A was located approaches the TU fixed point and merges with it. TU and U approach each other. (here $d_\parallel = 1.73$ and $d_\perp = 1.27$). Panel (f): TU and U have annihilated, so that the flow in the uniaxial case is always driven to the weak-coupling EWU. (here $d_\parallel = d_\perp = 1.5$).

APPENDIX B: RESCALING

As already noted in Ref. [29] the AKPZ equation can be rescaled such that either $\nu_\parallel = \nu_\perp$ or $|\lambda_\parallel| = |\lambda_\perp|$. The first variant is derived explicitly in this appendix, since the resulting rescaled AKPZ action is the one studied

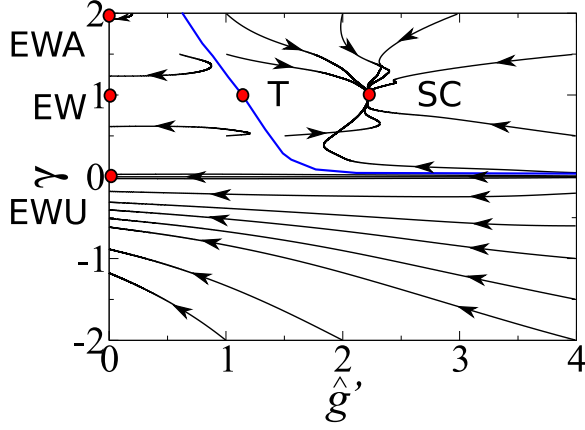


FIG. 6. (Color online) RG trajectories in the $(\hat{g}'_\kappa, \gamma'_\kappa)$ plane for $d_\parallel = 2$ and $d_\perp = 1$ in NLO approximation. The strong coupling SC fixed point is locally fully attractive. No A or U fixed points are present. Note that the position of the separatrix (highlighted in blue) is only roughly estimated.

throughout this work. Performing the substitution

$$h(t, \vec{x}) = \left(\frac{D}{\nu_\parallel}\right)^{1/2} \gamma^{d_\perp/4} h'(t', \vec{x}'), \quad (\text{A4a})$$

$$\tilde{h}(t, \vec{x}) = \left(\frac{\nu_\parallel}{D}\right)^{1/2} \gamma^{d_\perp/4} \tilde{h}'(t', \vec{x}'), \quad (\text{A4b})$$

$$\vec{x}_\parallel = \vec{x}'_\parallel, \quad \vec{x}_\perp = \gamma^{-1/2} \vec{x}'_\perp, \quad t = t'/\nu_\parallel, \quad (\text{A4c})$$

in the action Eq. (3b) where $\gamma = \nu_\parallel/\nu_\perp$, we obtain the rescaled AKPZ action (to simplify notations, the primes are omitted):

$$\begin{aligned} \mathcal{S}[h, \tilde{h}] = \int_{\mathbf{x}} \left\{ \tilde{h}(\mathbf{x}) \left(\partial_t h(\mathbf{x}) - \nabla_\parallel^2 h(\mathbf{x}) - \nabla_\perp^2 h(\mathbf{x}) \right. \right. \\ \left. \left. - \frac{\sqrt{g_b^\parallel}}{2} (\nabla_\parallel h(\mathbf{x}))^2 - \frac{\sqrt{g_b^\perp}}{2} (\nabla_\perp h(\mathbf{x}))^2 \right) - (\tilde{h}(\mathbf{x}))^2 \right\}. \end{aligned} \quad (\text{A5})$$

The rescaling therefore amounts to the substitution

$$\lambda_\parallel \rightarrow \left(\frac{\lambda_\parallel^2 D \gamma^{d_\perp/2}}{\nu_\parallel^3} \right)^{1/2} \equiv \sqrt{g_b^\parallel}, \quad (\text{A6a})$$

$$\lambda_\perp \rightarrow \left(\frac{\lambda_\perp^2 D \gamma^{d_\perp/2+2}}{\nu_\parallel^3} \right)^{1/2} \equiv \sqrt{g_b^\perp} \quad (\text{A6b})$$

in the original AKPZ action with all the other constants set to unity.

APPENDIX C: FLOW INTEGRALS FOR THE ANOMALOUS DIMENSIONS

In the NLO approximation, the flow integrals with zero external frequency and momentum are

where

$$\hat{k}_\kappa(\hat{q}_\parallel, \hat{q}_\perp) = \hat{f}_\kappa^D(\hat{q}_\parallel, \hat{q}_\perp) + r(\hat{q}^2), \quad (\text{A8a})$$

$$\hat{l}_\kappa(\hat{q}_\parallel, \hat{q}_\perp) = \hat{q}^2(\hat{f}_\kappa^\nu(\hat{q}_\parallel, \hat{q}_\perp) + r(\hat{q}^2)), \quad (\text{A8b})$$

$$\hat{q}^2 = \hat{q}_\parallel^2 + \hat{q}_\perp^2. \quad (\text{A8c})$$

The flow integrals in the LPA' approximation are easily deduced from the above NLO expressions by setting the flowing functions to one according to Eq. (38). Using the substitution $\hat{q}_\parallel = \hat{q} \cos \theta$, $\hat{q}_\perp = \hat{q} \sin \theta$ the double integrals in Eqs. (A7) can be further simplified to simple radial integrals

$$\int_0^\infty d\hat{q}_\parallel \hat{q}_\parallel^{d_\parallel-1} \int_0^\infty d\hat{q}_\perp \hat{q}_\perp^{d_\perp-1} \hat{I}(\hat{q}) = \frac{v_d}{v_{d_\parallel} v_{d_\perp}} \int_0^\infty d\hat{q} \hat{q}^{d-1} \hat{I}(\hat{q}), \quad (\text{A9a})$$

$$\int_0^\infty d\hat{q}_\parallel \hat{q}_\parallel^{d_\parallel+1} \int_0^\infty d\hat{q}_\perp \hat{q}_\perp^{d_\perp-1} \hat{I}(\hat{q}) = \frac{v_d d_\parallel}{v_{d_\parallel} v_{d_\perp} d} \int_0^\infty d\hat{q} \hat{q}^{d+1} \hat{I}(\hat{q}), \quad (\text{A9b})$$

where $\hat{I}(\hat{q})$ is a radial symmetric integrand.

In the isotropic case $\hat{f}^X(\hat{q}_\parallel, \hat{q}_\perp) \equiv \hat{f}^X(\hat{q})$ and $\gamma = 1$. One can then easily check that Eqs. (A7) with the help of Eq. (A9) simplify to the isotropic expressions (A4) in Refs. [47, 48], with

$$\hat{I}_\kappa^{D\nu} = \hat{I}_\kappa^{D\parallel} + \hat{I}_\kappa^{D\perp}, \quad (\text{A10a})$$

$$\hat{I}_\kappa^{\nu\nu} = \hat{I}_\kappa^{\parallel\parallel} + \hat{I}_\kappa^{\perp\perp} = \hat{I}_\kappa^{\perp\parallel} + \hat{I}_\kappa^{\parallel\perp}, \quad (\text{A10b})$$

$$\hat{I}_\kappa^{\nu 0} = \hat{I}_\kappa^{\parallel 0} = \hat{I}_\kappa^{\perp 0}, \quad \hat{I}_\kappa^{\nu D} = \hat{I}_\kappa^{\parallel D} = \hat{I}_\kappa^{\perp D}. \quad (\text{A10c})$$

APPENDIX D: ON THE NATURE OF THE ANISOTROPIC (A) FIXED POINT

We start with the β functions Eq. (30) in the perturbative limit Eq. (A2). As mentioned before, in the limit of small coupling \hat{g} the β functions coincide with the perturbative ones studied by TF [29]. Let us define $\epsilon = 2 - d$ with $\epsilon > 0$. For small ϵ and $\hat{g} \sim \mathcal{O}(\epsilon)$ the one-loop β functions become

$$\beta_{\hat{g}} = -\epsilon \hat{g} + \beta_0 \hat{g}^2 + \mathcal{O}(\epsilon^3), \quad (\text{A11a})$$

$$\beta_\gamma = \hat{g} \gamma (\gamma - 1) (2 - \Delta + \gamma(2 + \Delta)) A(d) + \mathcal{O}(\epsilon^2), \quad (\text{A11b})$$

where

$$\beta_0 = (8 - 16\Delta - 2\Delta^2 - 4\gamma(8 - 2\Delta - \Delta^2) + \gamma^2(2 - \Delta)^2) A(d).$$

The β_γ function has three zeros (see Sec. III): $\gamma_* = 1$ (isotropic case), $\gamma_* = 0$ (unitary case) and $\gamma_* = (\Delta - 2)/(\Delta + 2)$ (anisotropic case). Substituting the anisotropic fixed point value for γ into the first β function Eq. (A11a) we obtain

$$\beta_A(\hat{g}) = -\epsilon \hat{g} + \frac{8A(d)(4 - 5(d - 2d_\parallel)^2)}{(d - 2(1 + d_\parallel))^2} \hat{g}^2 + \mathcal{O}(\epsilon^3). \quad (\text{A12})$$

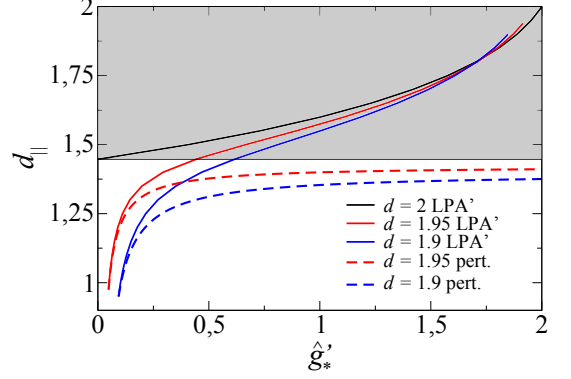


FIG. 7. (Color online) Coupling constant \hat{g}'_* at the anisotropic A fixed point close to $d = 2$ for different values of the sector dimension d_\parallel . The LPA' results are obtained from a numerical solution of the NPRG flow equations and perturbative results (labeled as pert.) from the one-loop expression Eq. (A13). For $d < 2$ and small d_\parallel the A fixed point is weak coupling and is well described by a perturbative treatment. For larger values of d_\parallel the A fixed point becomes strong coupling and the perturbative treatment is no longer justified. The sector dimension $d_\parallel = 1 + 1/\sqrt{5} \approx 1.45$ stands as the boundary beyond which the one-loop treatment for A breaks down, separating the weak coupling (white) from the strong coupling regime (shaded in grey).

This function has the nontrivial fixed point

$$\hat{g}'_* = -\frac{v_d}{4A(d)} \frac{(d-2)(d-2(1+d_\parallel))^2}{8(4-5(d-2d_\parallel)^2)}. \quad (\text{A13})$$

In order to stay in the perturbative regime where $\hat{g}_* \sim \mathcal{O}(\epsilon)$ is valid, the dimension d_\parallel has to verify $d_\parallel < 1 + 1/\sqrt{5}$. For $d < 2$ and depending on the splitting in the sector dimensions, the A fixed point therefore changes from weak coupling (for $d_\parallel < 1 + 1/\sqrt{5}$) to become strong coupling (for $d_\parallel \geq 1 + 1/\sqrt{5}$), see Fig. 7.

Let us mention that for $d_\parallel \geq 1 + 1/\sqrt{5}$ and $d \geq 2$ the perturbative treatment can be used in order to analyze the A fixed point as long as at least two loop contributions are included and $d_\parallel - 1 - 1/\sqrt{5} \sim \sqrt{\epsilon}$.

Finally, a similar analysis is possible for the uniaxial U fixed point. The critical sector dimension is $d_\parallel = \sqrt{5} - 1$ in that case.

APPENDIX E: GAUGE SYMMETRY OF THE UNIAXIAL AKPZ EQUATION

The AKPZ action in the uniaxial case ($\gamma = 0$) is invariant under the generalized gauged shift

$$h'(t, \vec{x}) = h(t, \vec{x}) + f(t, \vec{x}_\perp), \quad (\text{A14})$$

except for the two terms

$$\delta S = \int_{\mathbf{x}} \left\{ \tilde{h}(\mathbf{x}) (\partial_t f(t, \vec{x}_\perp) - \nu_\perp \nabla_\perp^2 f(t, \vec{x}_\perp)) \right\}, \quad (\text{A15})$$

which variation is linear in the field. Following the same line of reasoning as Ref. [46], one deduces that

$$\int_{\vec{x}_\parallel} \frac{\delta \Gamma}{\delta h} = \int_{\vec{x}_\parallel} \frac{\delta S}{\delta h} = 0, \quad (\text{A16})$$

or equivalently

$$\Gamma^{(n,m)}(\vec{p}_\parallel = 0, \dots) = (i\omega + \nu_\perp p_\perp^2) \delta_{m1} \delta_{n1}. \quad (\text{A17})$$

This implies that $\eta_\kappa^\perp = 0$ since ν_κ^\perp is not renormalized during the flow.

-
- [1] M. Kardar, G. Parisi, and Y.-C. Zhang, *Phys. Rev. Lett.* **56**, 889 (1986).
- [2] T. Halpin-Healy and Y.-C. Zhang, *Phys. Rep.* **254**, 215 (1995).
- [3] J. Krug, *Adv. Phys.* **46**, 139 (1997).
- [4] A. L. Barabási and H. E. Stanley, *Fractal Concepts in Surface Growth* (Cambridge University Press, Cambridge, U.K., 1995).
- [5] M. Kulkarni and A. Lamacraft, *Phys. Rev. A* **88**, 021603 (2013).
- [6] V. N. Gladilin, K. Ji, and M. Wouters, *Phys. Rev. A* **90**, 023615 (2014).
- [7] J. Villain, *J. Phys. I (France)* **1**, 19 (1991).
- [8] D. E. Wolf, *Phys. Rev. Lett.* **67**, 1783 (1991).
- [9] L. Chen and J. Toner, *Phys. Rev. Lett.* **111**, 088701 (2013).
- [10] E. Altman, L. M. Sieberer, L. Chen, S. Diehl, and J. Toner, [arXiv:1311.0876 \[cond-mat.stat-mech\]](https://arxiv.org/abs/1311.0876) (2013).
- [11] M. Prähofer and H. Spohn, *J. Stat. Phys.* **115**, 255 (2004).
- [12] T. Sasamoto, *J. Phys. A: Math. Gen.* **38**, L549 (2005).
- [13] T. Sasamoto and H. Spohn, *J. Stat. Mech.* **2010**, P11013 (2010).
- [14] P. Calabrese and P. Le Doussal, *Phys. Rev. Lett.* **106**, 250603 (2011).
- [15] G. Amir, I. Corwin, and J. Quastel, *Commun. Pure Appl. Math.* **64**, 466 (2011).
- [16] T. Imamura and T. Sasamoto, *Phys. Rev. Lett.* **108**, 190603 (2012).
- [17] I. Corwin, *Random Matrices* **01**, 1130001 (2012).
- [18] L.-H. Tang, B. M. Forrest, and D. E. Wolf, *Phys. Rev. A* **45**, 7162 (1992).
- [19] T. Ala-Nissila, T. Hjelt, J. Kosterlitz, and O. Venäläinen, *J. Stat. Phys.* **72**, 207 (1993).
- [20] C. Castellano, M. Marsili, M. A. Muñoz, and L. Pietronero, *Phys. Rev. E* **59**, 6460 (1999).
- [21] E. Marinari, A. Pagnani, and G. Parisi, *J. Phys. A: Math. Gen.* **33**, 8181 (2000).
- [22] F. D. A. Aarão Reis, *Phys. Rev. E* **69**, 021610 (2004).
- [23] S. V. Ghaisas, *Phys. Rev. E* **73**, 022601 (2006).
- [24] J. Kelling and G. Ódor, *Phys. Rev. E* **84**, 061150 (2011).
- [25] A. Pagnani and G. Parisi, *Phys. Rev. E* **87**, 010102 (2013).
- [26] T. Halpin-Healy, *Phys. Rev. Lett.* **109**, 170602 (2012).
- [27] T. Halpin-Healy, *Phys. Rev. E* **88**, 042118 (2013); *Phys. Rev. E* **88**, 069903(E) (2013).
- [28] T. J. Oliveira, S. G. Alves, and S. C. Ferreira, *Phys. Rev. E* **87**, 040102 (2013).
- [29] U. C. Täuber and E. Frey, *Europhys. Lett.* **59**, 655 (2002).
- [30] A. K. Chattopadhyay, *Phys. Rev. E* **76**, 050103 (2007).
- [31] A. Borodin and P. L. Ferrari, *J. Stat. Mech.* **2009**, P02009 (2009).
- [32] A. Borodin and P. L. Ferrari, *Commun. Math. Phys.* **325**, 603 (2014).
- [33] E. Vivo, M. Nicoli, and R. Cuerno, *Phys. Rev. E* **89**, 042407 (2014).
- [34] T. Halpin-Healy and A. Assdah, *Phys. Rev. A* **46**, 3527 (1992).
- [35] H. Jeong, B. Kahng, and D. Kim, *Phys. Rev. Lett.* **71**, 747 (1993).
- [36] H.-J. Kim, I.-m. Kim, and J. M. Kim, *Phys. Rev. E* **58**, 1144 (1998).
- [37] M. Prähofer and H. Spohn, *J. Stat. Phys.* **88**, 999 (1997).
- [38] H. Jeong, B. Kahng, and D. Kim, *Phys. Rev. E* **52**, R1292 (1995).
- [39] S. Mukherji and S. M. Bhattacharjee, *Phys. Rev. Lett.* **79**, 2502 (1997).
- [40] Y. Jung, K. Park, H.-J. Kim, and I.-m. Kim, *Phys. Rev. E* **62**, 1893 (2000).
- [41] G. Tang and B. Ma, *Physica A* **310**, 1 (2002).
- [42] G. Tang and B. Ma, *Int. J. Mod. Phys. B* **16**, 563 (2002).
- [43] T. Hwa, *Phys. Rev. Lett.* **69**, 1552 (1992).
- [44] L.-H. Tang, M. Kardar, and D. Dhar, *Phys. Rev. Lett.* **74**, 920 (1995).
- [45] L. Canet, H. Chaté, B. Delamotte, and N. Wschebor, *Phys. Rev. Lett.* **104**, 150601 (2010).
- [46] L. Canet, H. Chaté, B. Delamotte, and N. Wschebor, *Phys. Rev. E* **84**, 061128 (2011); *Phys. Rev. E* **86**, 019904(E) (2012).
- [47] T. Kloss, L. Canet, and N. Wschebor, *Phys. Rev. E* **86**, 051124 (2012).
- [48] T. Kloss, L. Canet, B. Delamotte, and N. Wschebor, *Phys. Rev. E* **89**, 022108 (2014).
- [49] B. Delamotte, in *Renormalization Group and Effective Field Theory Approaches to Many-Body Systems*, edited by J. Polonyi and A. Schwenk, Lecture Notes in Physics (Springer, Berlin, 2012); [arXiv:cond-mat/0702365](https://arxiv.org/abs/cond-mat/0702365) (2007).
- [50] H.-K. Janssen, *Z. Phys. B* **23**, 377 (1976); de Dominicis, C., *J. Phys. (Paris) Colloq.* **37**, 247 (1976).
- [51] P. C. Martin, E. D. Siggia, and H. A. Rose, *Phys. Rev. A* **8**, 423 (1973).

- [52] V. V. Lebedev and V. S. L'vov, *Phys. Rev. E* **49**, R959 (1994).
- [53] E. Frey, U. C. Täuber, and T. Hwa, *Phys. Rev. E* **53**, 4424 (1996).
- [54] J. Berges, N. Tetradis, and C. Wetterich, *Phys. Rep.* **363**, 223 (2002).
- [55] P. Kopietz, L. Bartosch, and F. Schütz, *Introduction to the Functional Renormalization Group*, Lecture Notes in Physics (Springer, Berlin, 2010).
- [56] L. Canet, B. Delamotte, O. Deloubrière, and N. Wschebor, *Phys. Rev. Lett.* **92**, 195703 (2004).
- [57] L. Canet, H. Chaté, and B. Delamotte, *J. Phys. A: Math. Theor.* **44**, 495001 (2011).
- [58] T. Kloss and P. Kopietz, *Phys. Rev. B* **83**, 205118 (2011).
- [59] J. Berges and D. Mesterházy, *Nucl. Phys. B Proc. Suppl.* **228**, 37 (2012).
- [60] C. Wetterich, *Phys. Lett. B* **301**, 90 (1993).
- [61] J.-P. Blaizot, R. Méndez-Galain, and N. Wschebor, *Phys. Lett. B* **632**, 571 (2006).
- [62] F. Benitez, J.-P. Blaizot, H. Chaté, B. Delamotte, R. Méndez-Galain, and N. Wschebor, *Phys. Rev. E* **85**, 026707 (2012).
- [63] B. Delamotte, Y. Holovatch, D. Ivaneyko, D. Mouhanna, and M. Tissier, *J. Stat. Mech.* **2008**, P03014 (2008).
- [64] We use $\alpha = 10$ in $d = 4$, compare Ref. [48].
- [65] In both cases ($d_{\parallel} = 3$ and $d_{\perp} = 1$) and ($d_{\parallel} = d_{\perp} = 2$) the fixed point TA ($\gamma_* > 1$) has crossed T ($\gamma_* = 1$) so that T and TA have interchanged their stability in γ -direction. In contrast, for $d = 3$ we find $\gamma_* < 1$ for TA. For the flow diagram this is however of minor importance since both fixed points T and TA are unstable so that the RG trajectories in ($d_{\parallel} = 3$ and $d_{\perp} = 1$) are almost similar to the situation ($d_{\parallel} = 2.5$ and $d_{\perp} = 0.5$) and ($d_{\parallel} = d_{\perp} = 2$) is almost similar to ($d_{\parallel} = 1.73$ and $d_{\perp} = 1.27$).